CHATTERING-FREE SLIDING MODE CONTROL FOR PROPELLANTLESS RENDEZ-VOUS USING DIFFERENTIAL DRAG

Hancheol Cho, Lamberto Dell'Elce, Gaëtan Kerschen

University of Liège, Space Structures & Systems Laboratory,
1, Chemin des Chevreuils, Liège B-4000, Belgium, Tel.: +32 4366 9449,
hancheol.cho@ulg.ac.be, lamberto.dellelce@ulg.ac.be, g.kerschen@ulg.ac.be

ABSTRACT

This paper develops a differential drag-based sliding mode controller for satellite rendez-vous. It is chattering-free and avoids bang-bang type control to adjust the relative motion more efficiently. In spite of uncertain nonlinear perturbations and disturbances, it is shown that the in-plane relative motion between two satellites can be effectively controlled by regulating the drag difference. An adaptive tuning rule is also presented such that the errors are suppressed to lie within a desired error box. The proposed controller is simple and easy to implement in a small satellite, and numerical simulations are carried out to demonstrate its effectiveness in a high fidelity environment.

Index Terms— Rendez-vous, Differential drag, Adaptive sliding mode control, Chattering

1. INTRODUCTION

Owing to the well-established correlation between spacecraft mass and mission's cost, there is great interest in fuel-optimal relative maneuvers between two or more satellites. In this context, the exploitation of natural perturbations is an attractive means to reduce or even remove fuel consumption, and hence, propellantless maneuvers using solar sail [1], geomagnetic field [2], Coulomb forces [3], and atmospheric drag were proposed. Amongst them, the idea to use differential drag as control force for relative motion is particularly attractive to enhance the maneuverability of small satellites in low-Earth orbit, so that ongoing and forthcoming missions envisage this technique to achieve propellantless rendez-vous, cluster keeping, or constellation deployment, e.g., QARMAN [4], SAMSON [5], and Flock [6], respectively. The utilization of differential drag to control the relative motion of satellites was first proposed by Leonard [7]. Based on the linearized Hill-Clohessy-Wiltshire equations [8,9], a rendez-vous strategy was proposed in which the relative motion of the chaser around the target is decomposed into a mean and a harmonic component, which inspired numerous researchers thereafter [10-12]. Bevilacqua et al. [13] used a similar approach to include the secular effects of the second zonal harmonic (J_2) perturbation. They further devised an adaptive Lyapunov-based controller with bang-bang type to account for nonlinear unmodeled dynamics [14]. In [15], a simple proportional-integral-derivative controller was derived to maintain the along-track distance between the two satellites using differential drag. Since bang-bang control cannot easily be implemented in practice, Dell'Elce and Kerschen [16] developed a non bang-bang optimal controller via model predictive control and compared it with an existing analytical technique.

In this paper a new chattering-free sliding mode controller is developed to perform an optimal rendez-vous of two satellites in low-Earth orbit, exploiting differential drag as control force. The proposed controller is designed to successfully compensate for uncertainty effects and/or unmodeled dynamics associated with air drag and to account for practical limitations such as input saturation. Also, continuity of the control functions embedded in the controller guarantees no chattering, hence, non bang-bang type control is obtained. In addition, a simple adaptive law to accurately estimate uncertainty bounds and a control gain is introduced. The novel sliding mode controller with the adaptive law automatically updates the control gain in real time to have errors remain within a user-specified small region. Numerical simulations assuming a realistic scenario are used to validate the robustness and accuracy of the chattering-free sliding mode controller.

2. RENDEZ-VOUS USING DIFFERENTIAL DRAG

In the current paper, it is assumed that only in-plane control is considered for rendez-vous. It is known that the controllability of the differential drag in the out-of-plane direction is two orders of magnitude smaller even for highly inclined orbits [17], and hence, it is quite limited to control the out-of-plane motion solely using differential drag. The main purpose of this paper is to develop a *computationally simple and light* controller that is able to execute accurate *non bang-bang type control* for differential drag-based rendez-vous with low computational overhead, without knowing any information about uncertainties under which the satellites may experience.
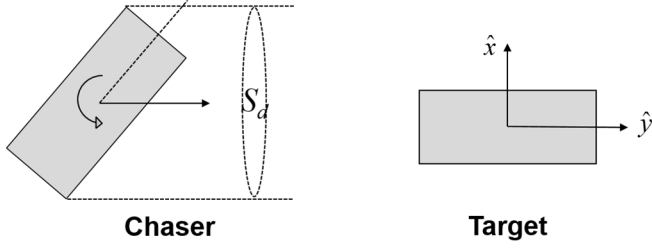
Figure 1 Scheme of attitude motion of chaser and target

Let us consider the rendez-vous problem illustrated in Figure 1. The target is assumed to have a stable attitude, while the chaser is controlled in real time by rotating about its orbital plane. The control output is S_d, the cross-sectional area of the chaser exposed to the atmosphere, and it is assumed that the drag of the chaser is proportional to S_d which is bounded by $S_d \in [S_{\min}, S_{\max}]$. A set of the input to the controller comprises

  1) estimates for the drag force and its uncertainty bounds obtained by the module 'drag estimator' and
  2) a reference trajectory computed by the module 'optimal maneuver planner',

and both 1) and 2) are evaluated once at the beginning of the maneuver. In this paper, 1) and 2) obtained in [16] are employed to design a sliding mode controller which shall be developed in Section 3.

The 'drag estimator' module undertakes the estimation of the drag force on the target and the chaser. The estimation is performed so that it minimizes the mean square errors between the observed and simulated semi-major axes of the satellites. Then, the differential drag is represented by [16]

$$\Delta F_d = F_{d,t}^{est} - F_{d,c}^{est} = F_{d,t}^{est}\left(1 - \frac{F_{d,c}^{est}}{F_{d,t}^{est}}\right)$$

$$= F_{d,t}^{est}\left[1 - \frac{C_{d,c}^{est} S_d}{C_{b,t}^{est} m_c}(1 + c_h x)\right], \qquad (1)$$

where S_d is the cross-sectional area of the chaser illustrated in Figure 1, m_c is the mass of the chaser, $F_{d,t}^{est}$ is the estimated time history of the drag of the target, $C_{d,c}^{est}$ is the estimated drag of the chaser, $C_{b,t}^{est}$ is the estimated ballistic coefficient of the target, c_h is the altitude correction factor, and x is the altitude gap between the target and the chaser. The output ($C_{b,t}^{est}$, $C_{d,c}^{est}$, $F_{d,t}^{est}$, c_h) of this module serves as the input to the 'optimal maneuver planner' and the sliding mode controller.

Next, the module 'optimal maneuver planner' computes the reference control output ($S_{d,r}$) and the reference trajectory ($x_r, y_r, \dot{x}_r, \dot{y}_r$) which are solved with an *hp*-adaptive Radau pseudospectral transcription [18] using the software GPOPS. To best balance between accuracy and computational efficiency, two dominant perturbations are included in this module: secular J_2 effects and short period / altitude-dependent variations of the drag.

It is noted that the coordinate system considered in this paper is the decomposed curvilinear system (x, y), which considerably improves the accuracy of the solution for middle and long range maneuvers. More specifically, x and y denote the radial and along-track position of the chaser with respect to the target, respectively, each of which comprises a mean (x_m, y_m) and an oscillatory component (x_o, y_o) so that $x_m + x_o = x$ and $y_m + y_o = y$. Schweighart and Sedwick [19] decomposed into these two components to account for the secular variations of the J_2 perturbations. More specifically, the two components satisfy the relations [16]:

$$x_m = \frac{4c^2}{2-c^2}x + \frac{2c}{(2-c^2)\omega}\dot{y},$$

$$y_m = y - \frac{2c}{(2-c^2)\omega}\dot{x},$$

$$\dot{x}_o = \frac{(2-c^2)\omega}{2c}y_o - \frac{2c}{(2-c^2)\omega}\Delta F_d, \qquad (2)$$

$$\dot{y}_o = -2\omega c x_o,$$

where ω is the orbital frequency of the target, $c = \sqrt{1 + \frac{3J_2 R_e^2}{8r_t^2}\left[1 + 3\cos(2i_t)\right]}$ is the Schweighart-Sedwick coefficient, while J_2 is the second zonal harmonic coefficient, R_e is the equatorial radius of the Earth, r_t is the distance from the center of the Earth to the target, and i_t is the inclination of the reference orbit of the target. The output ($S_{d,r}, x_r, y_r, \dot{x}_r, \dot{y}_r$) of this module then serves as an input to the controller.

3. CONTROLLER DESIGN

First, consider the ideal (reference) system on which the optimal reference control output ($S_{d,r}$) and the reference trajectory ($x_r, y_r, \dot{x}_r, \dot{y}_r$) are derived by the module 'optimal maneuver planner'. Since secular J_2 effects and short period

/ altitude-dependent variations of the drag are included, the following linearized equation of relative motion [19] holds:

$$\ddot{x}_r = 2\omega c \dot{y}_r + (5c-2)\omega^2 x_r,$$
$$\ddot{y}_r = -2\omega c \dot{x}_r + \Delta F_{d,r}, \qquad (3)$$

where $\Delta F_{d,r}$ is obtained by (1) and further rewritten using a *normalized* control u_r by

$$\Delta F_{d,r} = F_{d,t}^{est} \left[1 - \frac{C_{d,c}^{est} S_{d,r}}{C_{b,t}^{est} m_c} \left(1 + c_h x_r \right) \right] = \alpha_r u_r + \beta_r, \quad (4)$$

where the normalized control u_r is bounded by $u_r \in [0,1]$.

Next, we consider the real system that is assumed to be expressed in the form of

$$\ddot{x} = 2\omega c \dot{y} + (5c-2)\omega^2 x + g_x,$$
$$\ddot{y} = -2\omega c \dot{x} + \Delta F_d + g_y, \qquad (5)$$

where $g_x = g_x(t,x,y,\dot{x},\dot{y})$ and $g_y = g_y(t,x,y,\dot{x},\dot{y})$ are *unknown* perturbations and disturbances that compensate for *any differences* between the left hand sides and the right hand sides in (5). In addition, ΔF_d is given in (1) and further rewritten in the form:

$$\Delta F_d = F_{d,t}^{est} \left[1 - \frac{C_{d,c}^{est} S_d}{C_{b,t}^{est} m_c} \left(1 + c_h x \right) \right]$$
$$= (\alpha_r + \Delta\alpha) u + (\beta_r + \Delta\beta), \qquad (6)$$

where $\Delta\alpha$ and $\Delta\beta$ are *uncertain* additional terms, and $u \in [0,1]$.

Then, the error dynamics is described by

$$\ddot{e}_x = 2\omega c \dot{e}_y + (5c-2)\omega^2 e_x + g_x,$$
$$\ddot{e}_y = -2\omega c \dot{e}_x + \alpha_r \Delta u + (\Delta\alpha \cdot u + \Delta\beta + g_y), \qquad (7)$$

where $e_x = x - x_r$, $e_y = y - y_r$, $\Delta u = u - u_r$, and the terms g_x and $(\Delta\alpha \cdot u + \Delta\beta + g_y)$ are uncertain. The aim is to develop a control law Δu so that, upon applying it, the errors e_x and e_y converge to zero while suppressing the effects of the uncertainties. It should be noted that the control output u for the real system is given by $u = u_r + \Delta u$.

Now, define the 2-vector sliding surface $\mathbf{s} = \begin{bmatrix} s_x & s_y \end{bmatrix}^T$ of the form:

$$\mathbf{s} = \dot{\mathbf{e}} - \mathbf{S}\mathbf{e}, \qquad (8)$$

where $\mathbf{e} = \begin{bmatrix} e_x & e_y \end{bmatrix}^T$ and

$$\mathbf{S} = \begin{bmatrix} -2\zeta\sqrt{2-c^2}\,\omega & \dfrac{(2-c^2)\omega}{2c} \\ -2\omega c & 0 \end{bmatrix}, \qquad (9)$$

where ζ is a positive small constant. In order to guarantee the asymptotic stability, the real part of the eigenvalues of $\mathbf{S}$ should be negative, which is equivalent to the condition $\zeta > 0$. When $\mathbf{s} = \mathbf{0}$, (8) yields

$$\dot{e}_x = \frac{(2-c^2)\omega}{2c} e_y - 2\zeta\sqrt{2-c^2}\,\omega e_x,$$
$$\dot{e}_y = -2\omega c e_x. \qquad (10)$$

From (2), the errors on the mean components of the trajectory satisfy

$$e_{x,m} = \frac{4c^2}{2-c^2} e_x + \frac{2c}{(2-c^2)\omega} \dot{e}_y,$$
$$e_{y,m} = e_y - \frac{2c}{(2-c^2)\omega} \dot{e}_x, \qquad (11)$$

and if we substitute (10) into (11), we find that the mean component errors become

$$e_{x,m} = 0,$$
$$e_{y,m} = \frac{4\zeta c}{\sqrt{2-c^2}} e_x. \qquad (12)$$

Hence, if we choose a sufficiently small value for ζ, the mean component errors are identically zero in the x direction and very small in the y direction. Furthermore, (10) is analogous to the dynamics of the errors on the oscillatory components given by (2), and hence, the oscillatory component errors also progressively reduce to zero during the sliding phase $\mathbf{s} = \mathbf{0}$.

Next, the following Lyapunov function is defined as a prelude to controller design:

$$V = \frac{1}{2} \boldsymbol{s}^T \mathbf{P} \boldsymbol{s}, \tag{13}$$

where $\mathbf{P}$ is a constant positive definite matrix of the form:

$$\mathbf{P} = \begin{bmatrix} P_{11} & P_{12} \\ P_{21} & P_{22} \end{bmatrix}. \tag{14}$$

Since $\mathbf{P}$ is positive definite, its elements must satisfy

$$P_{11} > 0, \; P_{11}P_{22} > P_{12}P_{21}, \tag{15}$$

and $P_{22} > 0$ is further assumed in this paper. The derivative of (13) yields

$$
\begin{aligned}
\dot{V} &= \boldsymbol{s}^T \mathbf{P} \dot{\boldsymbol{s}} \\
&= \left(P_{11}s_x + P_{21}s_y \right) L^* + \left(P_{12}s_x + P_{22}s_y \right)\left(\alpha_r \Delta u + \Delta L \right) \\
&= \left(P_{12}s_x + P_{22}s_y \right)\left(\eta L^* + \alpha_r \Delta u + \Delta L \right) \\
&= \left(\frac{P_{12}}{P_{22}} s_x + s_y \right) P_{22} \left(\eta L^* + \alpha_r \Delta u + \Delta L \right),
\end{aligned}
\tag{16}
$$

where

$$
\begin{aligned}
L^* &= \left(5c^2 - 2 \right)\omega^2 e_x + 2\zeta\sqrt{2-c^2}\,\omega\dot{e}_y + \frac{\left(5c^2-2\right)\omega}{2c}\dot{e}_y, \\
\Delta L &= \Delta\alpha \cdot u + \Delta\beta + \eta g_x + g_y, \\
\eta &= \frac{P_{11}s_x + P_{21}s_y}{P_{12}s_x + P_{22}s_y}.
\end{aligned}
\tag{17}
$$

It is noted that L^* is measurable while ΔL is uncertain but bounded by $|\Delta L| \le L_M$ with L_M being a positive constant. When $P_{12}s_x + P_{22}s_y$ is zero, η is not defined and $\dot{V} = \left(P_{11}s_x + P_{21}s_y \right) L^*$ holds from (16), meaning that there is no control authority. This uncontrollability is instantaneous so at this instant we simply maintain Δu with its previous value (instead of using the control law which shall be given by (18)). Hence, in the development that follows it is assumed that $P_{12}s_x + P_{22}s_y$ is not zero and η is well defined.

Next, let us consider the following form of the control law:

$$\Delta u = -\frac{\Gamma}{\alpha_r}\left(\frac{P_{12}}{P_{22}} s_x + s_y \right) - \frac{\eta L^*}{\alpha_r}, \tag{18}$$

where the gain Γ is a positive constant. Substituting (18) into (16) yields

$$
\begin{aligned}
\dot{V} &= \left(\frac{P_{12}}{P_{22}} s_x + s_y \right) P_{22} \left[\Delta L - \Gamma \left(\frac{P_{12}}{P_{22}} s_x + s_y \right) \right] \\
&\le \left| \frac{P_{12}}{P_{22}} s_x + s_y \right| P_{22} L_M - P_{22}\Gamma \left(\frac{P_{12}}{P_{22}} s_x + s_y \right)^2.
\end{aligned}
\tag{19}
$$

Now, consider the region where $\left| \frac{P_{12}}{P_{22}} s_x + s_y \right| > \varepsilon$ holds, where ε is a small positive constant. Then, (19) further satisfies

$$
\begin{aligned}
\dot{V} &< \left| \frac{P_{12}}{P_{22}} s_x + s_y \right| P_{22} L_M - \varepsilon P_{22}\Gamma \left| \frac{P_{12}}{P_{22}} s_x + s_y \right| \\
&= \left| \frac{P_{12}}{P_{22}} s_x + s_y \right| P_{22} \left(L_M - \varepsilon\Gamma \right).
\end{aligned}
\tag{20}
$$

In order to guarantee the asymptotical stability of the system, $\dot{V}$ should be negative so that the gain Γ can be chosen as

$$\Gamma = \frac{L_M}{\varepsilon}. \tag{21}$$

In brief, it is shown that the control law given by (18) forces the trajectory of the error dynamics (7) to move from initial conditions to the region $\left| \frac{P_{12}}{P_{22}} s_x + s_y \right| \le \varepsilon$ in a finite time and remain in the region.

The only concern is now how to determine the gain Γ because it requires the prior knowledge about the uncertainty bound L_M. In practice, it is very difficult to accurately estimate the bound value. Hence, an adaptive law that automatically tunes the uncertain parameter Γ is proposed.

First, we know that if the gain Γ given by (21) is applied, the system is eventually bounded by $\left| \frac{P_{12}}{P_{22}} s_x + s_y \right| \le \varepsilon$. Next, if we assume that the gain 2Γ is applied to the system, then $\left| \frac{P_{12}}{P_{22}} s_x + s_y \right| \le \frac{\varepsilon}{2}$ would be obtained because from (21) increasing Γ twice is mathematically equivalent to decreasing the value of ε by half. In general, if the estimated gain $\hat{\Gamma}$ is applied, the

system is bounded by $\left|\dfrac{P_{12}}{P_{22}}s_x+s_y\right|\le\varepsilon\dfrac{\Gamma}{\hat{\Gamma}}=\hat{\varepsilon}$, where Γ is the real (unknown) gain. This observation provides us with a new method to determine the gain Γ. Suppose that we apply a rough estimate $\hat{\Gamma}$ and observe $\left|\dfrac{P_{12}}{P_{22}}s_x+s_y\right|\le\hat{\varepsilon}$. Then, the real gain Γ can be estimated by

$$\Gamma=\frac{\hat{\varepsilon}}{\varepsilon}\hat{\Gamma}, \qquad (22)$$

where $\hat{\Gamma}$ is the tried estimate for the gain, and $\hat{\varepsilon}$ and ε are the observed and the desired upper bound for $\left|\dfrac{P_{12}}{P_{22}}s_x+s_y\right|$, respectively. Now, we have the following adaptive law for the gain Γ:

<u>Adaptive Law:</u> Let Γ_0 be the initial estimate. Then, the real-time adaptive law for the gain Γ is given by the following rules:

1) At each instant of time $\left|\dfrac{P_{12}}{P_{22}}s_x+s_y\right|$ is compared with ε. When $\left|\dfrac{P_{12}}{P_{22}}s_x+s_y\right|\le\varepsilon$, Γ maintains its current value (with Γ_0 as the initial condition). In discrete time implementation, it is expressed as

$$\Gamma^{(k+1)}=\Gamma^{(k)}, \quad\text{when } \left|\frac{P_{12}}{P_{22}}s_x^{(k)}+s_y^{(k)}\right|\le\varepsilon, \quad (23)$$

where the superscript (k) denotes a quantity at the kth scan time.

2) If $\left|\dfrac{P_{12}}{P_{22}}s_x+s_y\right|>\varepsilon$ at time t, then the gain Γ should be updated to be multiplied by $\left|\dfrac{P_{12}}{P_{22}}s_x+s_y\right|/\varepsilon$. In discrete time implementation, it is represented by

$$\Gamma^{(k+1)}=\Gamma^{(k)}\frac{\left|\dfrac{P_{12}}{P_{22}}s_x^{(k)}+s_y^{(k)}\right|}{\varepsilon}, \quad\text{when } \left|\frac{P_{12}}{P_{22}}s_x^{(k)}+s_y^{(k)}\right|>\varepsilon. \quad (24)$$

In order to prevent a sudden rise of the gain, (24) is relaxed by imposing a rate limiter δ:

$$\Gamma^{(k+1)}=\Gamma^{(k)}\cdot\min\left(\delta,\frac{\left|\dfrac{P_{12}}{P_{22}}s_x^{(k)}+s_y^{(k)}\right|}{\varepsilon}\right), \quad (25)$$

where δ is a positive constant. (25) limits the increasing rate of the gain by δ.

<u>Proof:</u> If $\left|\dfrac{P_{12}}{P_{22}}s_x+s_y\right|>\varepsilon$ is observed, it means that the current gain Γ is not enough to suppress $\left|\dfrac{P_{12}}{P_{22}}s_x+s_y\right|$ less than ε. By exploiting the adaptive law given by (25), the gain Γ gradually increases until the condition $\left|\dfrac{P_{12}}{P_{22}}s_x+s_y\right|\le\varepsilon$ is attained, which is guaranteed by (22). ❑

Finally, the final *normalized* control is obtained by $u=u_r+\Delta u$, where u_r is given in (4). Then, the *actual* control output S_d is retrieved using (6) and saturated to satisfy $S_d\in\left[S_{\min},S_{\max}\right]$. Since only continuous functions are included in u, S_d is also continuous and chattering free.

4. NUMERICAL SIMULATION

The new continuous controller with the adaptive law proposed in this paper is applied to a realistic scenario for rendez-vous. The chaser is QARMAN, a triple-unit CubeSat developed by the Von Karman Institute in Belgium. The University of Liège is in charge of developing a payload onboard QARMAN for the in-orbit validation of differential drag-based maneuvers. The target is another QB50 spacecraft flying with the long axis aligned to the orbital velocity.

The parameters used in the simulation are listed in Table 1. It is supposed that the real system associated with (5) includes gravitational perturbations up to order and degree 10, solar radiation pressure, luni-solar perturbations, and perturbations of the polar axis. The atmospheric model is NRLMSISE-00, and a 30% bias and short period stochastic variations, based on [20], are also included. Figure 2 illustrates real and estimated drag of the target.

The control parameters are selected as

$$\begin{aligned}
&L_M=10^{-5},\ \varepsilon=0.005,\ \zeta=10^{-4},\ \delta=1.01,\\
&P_{11}=3000,\ P_{12}=1000,\ P_{21}=0,\ P_{22}=10^6.
\end{aligned} \quad (26)$$

Table 1 Simulation parameters

Mean elements of the target	Semi-major axis	6728·10³ m
	Eccentricity	0
	Inclination	98 deg
	RAAN	90 deg
	Argument of perigee	0 deg
	True anomaly	0 deg
Initial gap of the chaser	Along-track	50·10³ m
	Radial	100 m
Target properties	Ballistic coefficient	0.014 m²kg⁻¹
Chaser properties	Mass	4 kg
	Dimensions	0.3×0.1×0.1 m³
	Drag coefficient	2.8
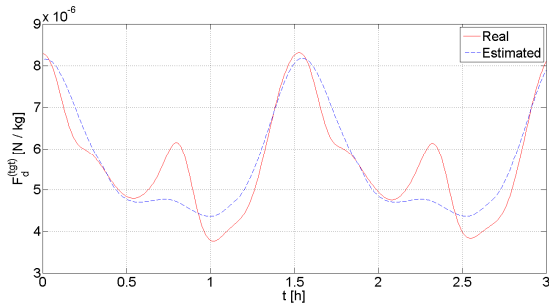
Figure 2 Real (red) and estimated (blue) drag of target

It is observed that if the initial gain is too large, the control output S_d is easily saturated and the errors start to oscillate with large amplitudes from the beginning of the maneuver. Hence, it is safe to try a small value for the initial guess of the gain. Then, it will be automatically tuned to gradually increase according to the adaptive law.

Figure 3 exhibits the planned and controlled trajectories in the *y-x* plane (left) and the final phase (right). The red solid lines represent the reference trajectories obtained by the module 'optimal maneuver planner' and the black dotted curves are associated with the controlled ones.

In Figure 4 the cross-sectional area of the chaser S_d is depicted. The red solid line represents the reference input

obtained by the 'optimal maneuver planner' and the black dotted curve is the control output. From the figure, one can observe that the control output S_d generally follows the reference $S_{d,r}$ while the tiny difference between them fights for reducing the uncertain effects. As a result, the controlled trajectory tracks the reference one quite well with bounded errors in both *x*- and *y*- axes. To see this boundedness more clearly, one can consider Figure 5, which depicts the time history of the errors in *x* and *y* directions. It is evident from the figure that the errors in both directions do not diverge but are bounded by $|e_x| \leq 20$ (m) and $|e_y| \leq 100$ (m) during the *whole* maneuver.

To see how the adaptive law works, refer to Figure 6. In the upper figure, the quantity $\frac{P_{12}}{P_{22}} s_x + s_y$ is plotted while the time history of the gain Γ is depicted in the lower figure. The two red horizontal lines are drawn in the upper figure to display $\pm \varepsilon$ and to stress that the quantity $\frac{P_{12}}{P_{22}} s_x + s_y$ eventually should lie between the two red horizontal lines. In the first half of the maneuver, $\frac{P_{12}}{P_{22}} s_x + s_y$ sometimes deviates from the bounded region $[-\varepsilon, +\varepsilon]$ and the gain increases on all such occasions by following the adaptive law. As a result, in the second half of the maneuver, $\frac{P_{12}}{P_{22}} s_x + s_y$ is bounded by the region and remains there. A further look at the figure reveals the fact that $\left| \frac{P_{12}}{P_{22}} s_x + s_y \right|$ is finally bounded by 0.0013 that is less than $\varepsilon = 0.005$, which means that the updated final gain value $\Gamma \simeq 0.056$ is larger than the real gain value that exactly enforces $\left| \frac{P_{12}}{P_{22}} s_x + s_y \right| \leq \varepsilon$. The reason for the excessive gain is resulted from *slow*
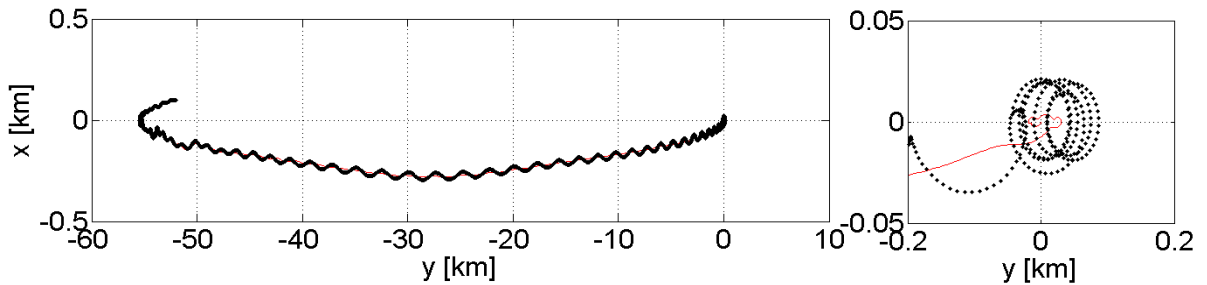
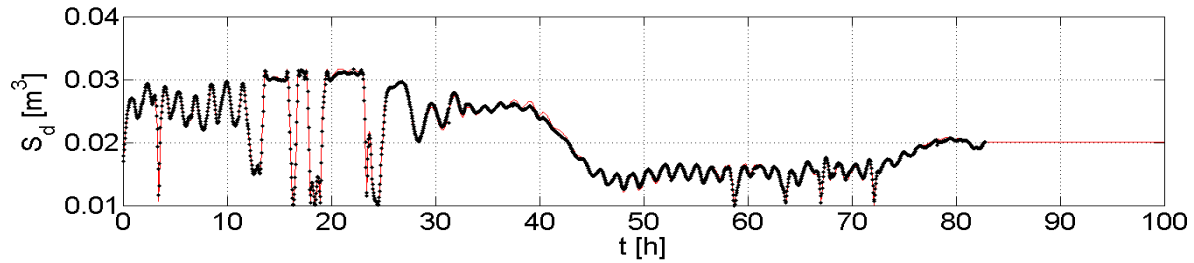**Figure 3 Global trajectories in *y-x* plane (left) and the final phase (right)**

Figure 4 Cross-sectional area of the chaser S_d

response of the differential drag-based controlled system. Hence, even if the gain value is enough, it takes time for the system to become bounded within the desired region and during the time interval, the adaptive law continuously increases the gain value. Our future work will account for this issue.

5. CONCLUSIONS

A new chattering-free sliding mode controller is proposed for rendez-vous of the two satellites only using differential drag. Unlike most of the literature that exploits the bang-bang control, it is continuous and enables fine control. Furthermore, the controller developed in this paper is computationally simple and light to be implemented onboard a real small CubeSat. In order to counteract the effects of unknown perturbations and disturbances, the adaptive law is presented that tunes the control gain in real time by which the gain gradually increases until the sliding variables or the errors are confined within a desired region. Numerical simulations with the realistic scenario validate the efficacy of the new adaptive sliding mode controller.

6. REFERENCES

[1] T. Williams and Z.S. Wang, "Uses of Solar Radiation Pressure for Satellite Formation Flying," *International Journal of Robust and Nonlinear Control*, Vol. 12, pp. 163-183, 2002.

[2] M.A. Peck, B. Streetman, C.M. Saaj, and V. Lappas, "Spacecraft Formation Flying Using Lorentz Forces," *Journal of the British Interplanetary Society*, Vol. 60, pp. 263-267, 2007.

[3] L.B. King, G.G. Parker, S. Deshmukh, and J.H. Chong, "Spacecraft Formation-flying Using Inter-vehicle Coulomb Forces," *Technical report*, Michigan Technological University, 2002.
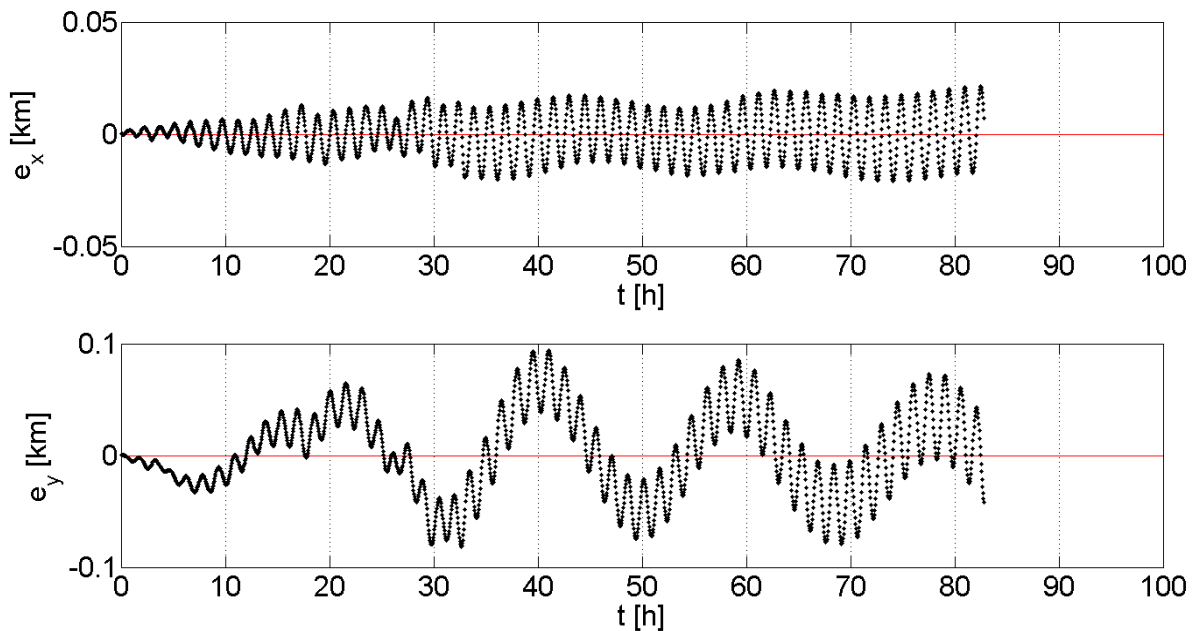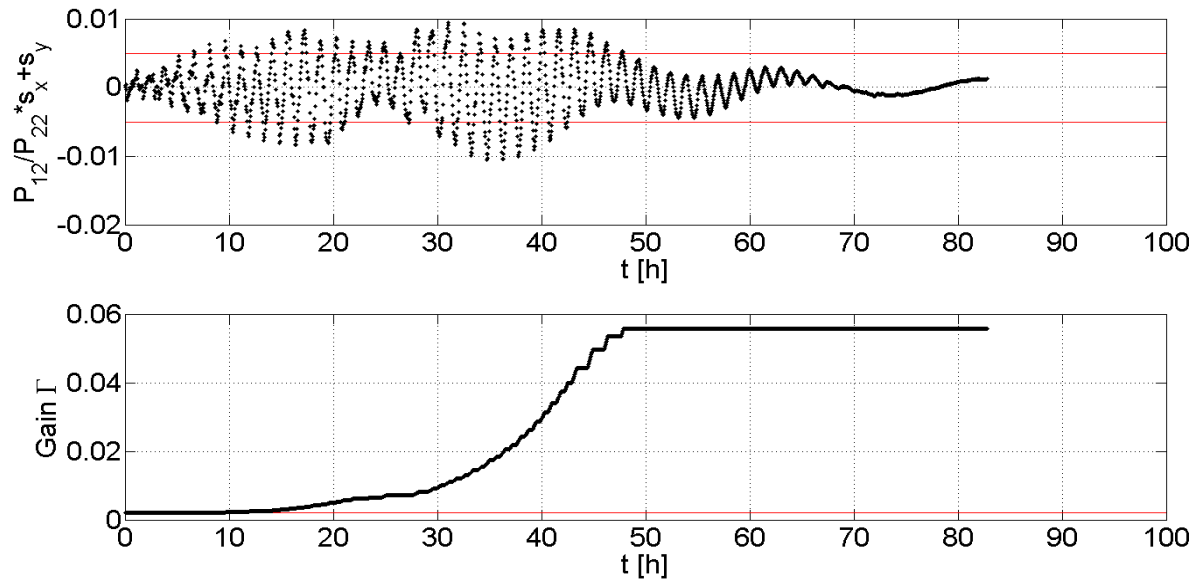
Figure 5 Errors in the *x*-axis (upper) and *y*-axis (lower)

Figure 6 $\dfrac{P_{12}}{P_{22}} s_x + s_y$ **(upper) and the gain** Γ **(lower) updated by the adaptive law**

[4] G. Bailet, I. Sakraker, T. Scholz, and J. Muylaert, "Qubesat for Aerothermo-dynamic Research and Measurement on AblatioN," *4th International ARA Days*, Arcachon, France, 2013.

[5] P. Gurfil, J. Herscovitz, and M. Pariente, "The SAMSON Project - Cluster Flight and Geolocation with Three Autonomous Nano-satellites," *28th Annual AIAA/USU Conference on Small Satellites*, Logan, USA, 2012.

[6] C.R. Boshuizen, J. Mason, P. Klupar, and S. Spanhake, "Results from the Planet Labs Flock Constellation," *28th Annual AIAA/USU Conference on Small Satellites*, Logan, USA, 2014.

[7] C.L. Leonard, "Formationkeeping of Spacecraft via Differential Drag," *M.Sc. Thesis*, Massachusetts Institute of Technology, Cambridge, 1986.

[8] G.W. Hill, "Researches in the Lunar Theory," *American Journal of Mathematics*, Vol. 1, pp. 5–26, 1878.

[9] W.H. Clohessy and R.S. Wiltshire, "Terminal Guidance System for Satellite Rendezvous," *Journal of Aerospace Sciences*, Vol. 27, pp. 653–658, 1960.

[10] G.B. Palmerini, S. Sgubini, and G. Taini, "Spacecraft Orbit Control Using Air Drag," Paper IAC-05-c1.6.10, 2005.

[11] M. Mathews and S. Leszkiewicz, "Efficient Spacecraft Formationkeeping with Consideration of Ballistic Control," *AIAA AA-88-0375*, 1988.

[12] P. Gurfil and N.J. Kasdin, "Nonlinear Low-thrust Lyapunov-based Control of Spacecraft Formations," *American Control Conference*, Denver, USA, pp. 1758—1763, June 2003.

[13] R. Bevilacqua and M. Romano, "Rendezvous Maneuvers of Multiple Spacecraft Using Differential Drag under J_2 Perturbation," *Journal of Guidance, Control, and Dynamics*, Vol. 31, pp. 1595-1607, 2008.

[14] D. Pérez and R. Bevilacqua, "Differential Drag Spacecraft Rendezvous Using an Adaptive Lyapunov Control Strategy," *Acta Astronautica*, Vol. 83, pp. 196-207, 2013.

[15] B.S. Kumar, A. Ng, K. Yoshihara, and A.D. Ruiter, "Differential Drag as a Means of Spacecraft Formation Control," *IEEE Transactions on Aerospace and Electronic System*, Vol. 47, pp. 1125-1135, 2011.

[16] L. Dell'Elce and G. Kerschen, "Optimal Propellantless Rendez-vous Using Differential Drag," *Acta Astronautica*, Vol. 109, pp. 112-123, 2015.

[17] O. Ben-Yaacov and P. Gurfil, "Stability and Performance of Orbital Elements Feedback for Cluster Keeping Using Differential Drag," *The Journal of the Astronautical Sciences*, Vol. 61, pp. 198-226, 2014.

[18] D. Garg, M.A. Patterson, W.W. Hager, A.V. Rao, D.A. Benson, and G.T. Huntington, "A Unified Framework for the Numerical Solution of Optimal Control Problems Using Pseudospectral Methods," *Automatica*, Vol. 46, pp. 1843-1851, 2010.

[19] S.A. Schweighart and R.J. Sedwick, "High-fidelity Linearized J_2 Model for Satellite Formation Flight," *Journal of Guidance, Control, and Dynamics*, Vol. 25, pp. 1073–1080, 2002.

[20] M. Zijlstra and S. Theil, "Model for Short-term Atmospheric Density Variations," *Earth Observation with CHAMP*, Springer Berlin Heidelberg, 2005.